Solitary waves in a non-integrable FPU chain

Lev Truskinovsky
LMS, CNRS-UMR 7649, École Polytechnique, Route de Saclay, 91128 Palaiseau, France

Anna Vainchtein
Department of Mathematics, University of Pittsburgh, Pittsburgh, PA 15260, USA

(Dated: September 13, 2014)

We present a new family of exact solutions describing discrete solitary waves in a non-integrable Fermi-Pasta-Ulam chain. The family is sufficiently rich to cover the whole spectrum of known behaviors from delocalized quasicontinuum waves moving with near-sonic velocities, to highly localized anticontinuum excitations with only one particle moving at a time.

PACS numbers: 05.45.Yv,45.50.-j,46.40.Cd

I. INTRODUCTION

Solitary waves in lattices, represented by homoclinic traveling wave trajectories of discrete dynamical systems, play a crucial role in many areas of science from condensed matter theory to biophysics [1]. In *integrable* systems solitary waves, known as solitons or quasiparticles, are understood rather thoroughly, with Toda lattice being the most prominent example that covers the whole range of possible behaviors from weak quasicontinuum (QC) waves in almost harmonic chains, to strong anticontinuum (AC) waves in chains of rigid disks [2]. However, quasiparticles in integrable systems do not interact during collisions, which excludes, for instance, finite thermal conductivity. Therefore integrable systems cannot be used as a generic description of localized excitations, and the challenge is to find a *non-integrable* equivalent of the Toda lattice allowing one to capture a similarly broad range of behaviors.

Most of our theoretical knowledge about solitary waves in non-integrable systems comes from the study of various quasicontinuum approximations which adequately describe weak excitations in elastic lattices [3, 4] and slow waves in granular chains [5] but fail in a generic AC limit. Solitary waves in general Fermi-Pasta-Ulam (FPU) lattices have been studied mostly numerically [6] or using qualitative asymptotic methods [7]. Some exact solutions were obtained for special classes of potentials [8] which were too narrow to describe the QC $\to$ AC crossover.

In this paper we construct a family of exact solitary wave solutions for a parametric non-integrable FPU problem with piecewise quadratic energy [9]. This class of energies can be viewed as an analytically transparent approximation of general FPU potentials. We treat nonlinearity as inhomogeneity [10, 11] and show that for this class of potentials the problem of finding solitary wave solutions reduces to a linear integral equation plus a nonlinear algebraic equation. We solve the integral equation using the Wiener-Hopf technique and express the solution as a combination of linear waves whose phase speeds are equal to the speed of the solitary wave. Truncations of the ensuing series, involving progressively decreasing wavelengths, generate converging approximations that are fully explicit.

The importance of the obtained family of solutions is clear from the fact that it can be used as a non-integrable interpolant between two integrable limits: weak KdV-type QC solitary waves [12, 13] and high-energy strongly discrete AC solitary waves [14, 15]. Our numerical results indicate that the members of the crossover family exhibit (weakly) inelastic interactions and that their stability is controlled by the sign of the derivative of the energy-velocity relation. We also show that the simplest long-wave truncation of the obtained series provides a much better overall quasicontinuum approximation of the discrete solution than the conventional quasicontinuum theories based on either Taylor [16] or Padé [17, 18] approximations.

The remainder of the paper is organized as follows. In Sec. II we formulate the problem and introduce the piecewise quadratic potential. The main ideas involved in the construction of the solitary wave solutions are presented in Sec. III, where we also briefly discuss some numerical results on stability and collision of the solitary waves. In Sec. IV we compare the simplest long-wave approximation of the constructed solution to the more conventional quasicontinuum models and discuss the low-energy KdV-type limit. The strongly discrete AC limit is presented in Sec. V. Sec. VI summarizes our findings. The two Appendices contain the results of more technical nature, including the details of the derivation of the solitary wave solution (Appendix A) and numerical study of its stability (Appendix B).

II. PROBLEM FORMULATION

The dimensionless energy of the FPU chain can be written as

$$\mathcal{H} = \sum_{j=-\infty}^{\infty} \left[\frac{1}{2}\dot{u}_j^2 + \phi(u_j - u_{j-1}) \right], \tag{1}$$

where $u_j(t)$ is the displacement of a mass point and $\phi(w)$ is the interaction potential. In strain variables $y_j = u_j -$

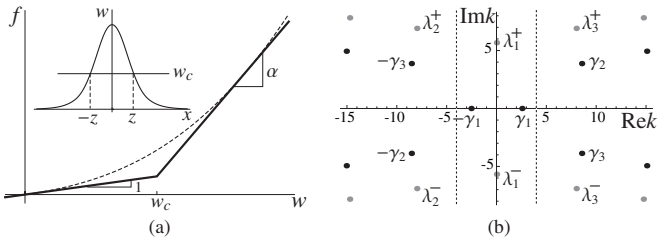

FIG. 1. (a) Bilinear approximation (bold curve) of a generic smooth force-strain relation (dashed curve). Inset shows a schematic structure of the solitary wave. (b) The structure of nonzero roots of $L(k) = 0$ (gray circles) and $G(k) = 0$ (black circles) at $V = 3$ and $\alpha = 16$. The simplest approximation with $n = 1$ includes the roots $\pm\gamma_1$ and $\lambda_1^{\pm}$ located within the strip $|\mathrm{Re}k| < l_1$ marked by the dashed lines. The next approximation with $n = 3$ also includes the roots $\pm\gamma_{2,3}$ and $\lambda_{2,3}^{\pm}$.

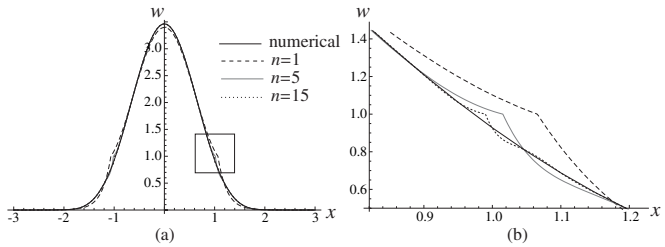

FIG. 2. (a) Several finite-root approximations of the solitary wave at $V = 3$, $w_c = 1$ and $\alpha = 16$ compared with the numerical solution of (6), (7). (b) The enlarged view of the solutions inside the rectangle in (a) around $w = w_c$.

u_{j-1} the traveling wave solution moving with velocity V has the form $y_j(t) = w(x)$, where $x = j - Vt$. The function $w(x)$ satisfies

$$V^2 w'' = f(w(x+1)) - 2f(w(x)) + f(w(x-1)), \quad (2)$$

where $f(w) = \phi'(w)$. Solitary waves are selected by the conditions at infinity: $w(x) \to 0$ at $|x| \to \infty$.

The main idea of our approximation is to replace the general potential $\phi(w)$ by a smooth piecewise quadratic function with bilinear derivative

$$f(w) = \begin{cases} w, & w \le w_c \\ \alpha(w - w_c) + w_c, & w \ge w_c. \end{cases} \quad (3)$$

In view of the invariance $f(w) \to -f(-w)$, $w \to -w(x)$, it suffices to consider the case $\alpha > 1$, as in Fig. 1a. One can show that the velocity of the solitary wave must be within the range $1 < V < \sqrt{\alpha}$.

III. SOLITARY WAVE SOLUTION

Due to the linearity of $f(w)$ at $w \neq w_c$ the solution of our boundary value problem can be written as a sum of plane waves with phase velocities equal to the velocity of the solitary wave. The corresponding wave numbers can be found from the characteristic equations

$$G(k) = 4\alpha \sin^2 \frac{k}{2} - V^2 k^2 = 0$$

at $|x| < z$, where we assume $w(x) > w_c$, and

$$L(k) = 4 \sin^2 \frac{k}{2} - V^2 k^2 = 0$$

at $|x| > z$, where $w(x) < w_c$. To find the amplitudes of the plane waves we write (cf. [19, 20])

$$f(w(x)) = w(x) + A \int_{-z}^{z} \theta(s - x) h(s) ds, \quad (4)$$

where $\theta(x)$ is the Heaviside function. We assume that the unknown function $h(x)$ representing the 'inhomogeneity' is odd and that it vanishes at $|x| > z$. It is also normalized via

$$\int_0^z h(s) ds = 1. \quad (5)$$

The ensuing linear problem for the 'inhomogeneous' material (4) yields the following relation between the Fourier transform $H(k) = \int_{-z}^{z} h(s) \exp(-iks) ds$ of $h(x)$ and $w(x)$:

$$w(x) = \frac{A}{2\pi i(\alpha - 1)} \int_{-\infty}^{\infty} \left(\frac{G(k)}{L(k)} - 1 \right) \frac{H(k)}{k} e^{ikx} dk. \quad (6)$$

Using (6) together with the consistency condition $Ah(x) = (1 - \alpha)w'(x)$ for $|x| < z$ that follows from (3), (4), we obtain the linear integral equation for $h(x)$:

$$(\alpha - 1) \int_{-z}^{z} q(x - s) h(s) ds + h(x) = 0, \quad |x| < z, \quad (7)$$

where

$$q(x) = \frac{1}{2\pi(\alpha - 1)} \int_{-\infty}^{\infty} \left(\frac{G(k)}{L(k)} - 1 \right) e^{ikx} dk.$$

The remaining nonlinear problem is to find z ensuring the existence of a nontrivial solution of (7). Once z and $h(x)$ are known, one can recover $w(x)$ from (6), with the multiplicative constant A determined from $w(z) = w_c$.

An explicit solution of (7) can be constructed using a variant of the Wiener-Hopf method [21–23]. Let λ_i^+ and λ_i^- be the roots of $L(k) = 0$ with positive and negative imaginary parts, respectively, and let γ_i denote the roots of $G(k) = 0$ with positive real parts [24]. Suppose that n roots γ_i and n roots λ_i^+ are located within a strip $|\mathrm{Re}k| < l_n$; such n is necessarily odd, and due to the symmetry of the roots the total number of the nonzero roots in the nth strip is $4n$; see Fig. 1b. Then

$$w(x) = \begin{cases} a_0 + \sum_{j=1}^{\infty} a_j \cos(\gamma_j x), & |x| \le z \\ \sum_{j=1}^{\infty} b_j \exp(i\lambda_j^+ |x|), & |x| \ge z, \end{cases} \quad (8)$$

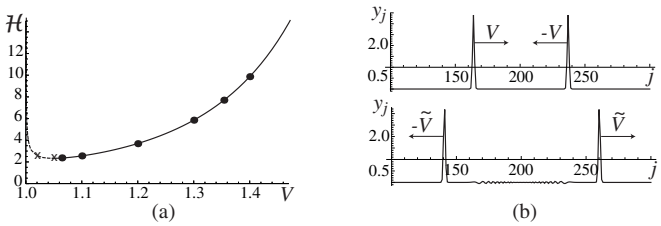

FIG. 3. (a) The energy of the solitary wave $\mathcal{H}$ as a function of V at $\alpha = 4$ and $w_c = 1$. The dashed portion of the curve corresponds to unstable waves. Circles and crosses mark velocities at which the solitary wave solutions were found stable and unstable, respectively, in the numerical simulations of (B1) with initial conditions (B2) or (B3); (b) Snapshots of two stable solitary waves before the collision (upper panel, $t = 30$, $V = 1.6$) and after the collision (lower panel, $t = 90$, $\tilde{V} \approx 1.6$).

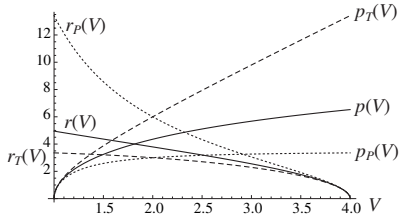

FIG. 4. The velocity dependence of the magnitudes r and p of real and purely imaginary roots of the characteristic equations in the discrete model (solid lines) and in Taylor (dashed) and Padé (dotted) quasicontinuum approximations. Here $\alpha = 16$.

where the coefficients a_j, b_j derived in Appendix A are given by (A13), (A14), (A15) as limits of expressions involving the roots of characteristic equations inside the nth strip. The derivation also yields the location of the transition point as $z = \lim_{n\to\infty} z_n$, where z_n is a solution of the algebraic equation $\det M_n(z_n) = 0$, with

$$(M_n)_{jm} = \gamma_j^{m-1}\left(\frac{(-1)^{m-1}e^{i\gamma_j z_n}}{\prod_{i=1}^{n}(\gamma_j - \lambda_i^-)} + \frac{e^{-i\gamma_j z_n}}{\prod_{i=1}^{n}(\gamma_j - \lambda_i^+)}\right). \quad (9)$$

Using the normalization condition (5), we obtain a unique approximation $w_n(x)$ of the solution (8) for each n; see Appendix A for details. The convergence of these approximations is illustrated in Fig. 2 (see also Fig. 8 in Appendix A). The 'corners' at $x = \pm z_n$ are the artifacts of the series truncation and disappear in the limit $n \to \infty$.

Stability and collision properties of the obtained solitary waves were studied numerically; see Appendix B for details. Our results, summarized in Fig. 3a, suggest that the instability condition is $d\mathcal{H}/dV < 0$, which is known as the Vakhitov-Kolokolov criterion [25, 26]. In view of the non-integrable nature of the system it is not surprising that a typical collision test for two stable solitary waves shows (slightly) inelastic interaction; see Fig. 3b. Additional stability and collision results are presented in Appendix B.

IV. QUASICONTINUUM APPROXIMATIONS

Consider now in more detail the simplest approximate solution $w_n(x)$ corresponding to $n = 1$. It involves four nonzero roots of the characteristic equations that are *closest* to $k = 0$ and therefore qualifies as a quasicontinuum (QC) approximation. Letting $\pm\gamma_1 = \pm r$ and $\lambda_1^{\pm} = \pm ip$ (see Fig. 1b), where r and p are positive real numbers, we obtain the following explicit representation:

$$w(x) = \frac{w_c}{\alpha - V^2}\left(\alpha - 1 + (V^2 - 1)\frac{\sqrt{p^2 + r^2}}{p}\cos rx\right) \quad (10)$$

for $|x| < z$ and

$$w(x) = w_c e^{-p(|x| - z)} \quad (11)$$

for $|x| > z$, with

$$z = \frac{1}{r}\left(\pi - \arctan\frac{r}{p}\right). \quad (12)$$

The typical dependence of p and r on V is shown in Fig. 4.

It is instructive to compare the underlying nonlocal QC theory with the more conventional local QC theories based on either Taylor or Padé approximations of the operator $\Lambda(k) = 4\sin^2(k/2)/k^2$ involved in the Fourier representation of (2) [16, 27]. The first-order Taylor expansion of $\Lambda(k)$ near $k = 0$ leads to the Boussinesq-type equation

$$u_{tt} = (f(u_\xi) + (1/12)(f(u_\xi))_{\xi\xi})_\xi \quad (13)$$

for the displacement field $u(\xi, t)$. The solitary wave solution of (13) is given again by (10)-(12) but with $r = \sqrt{12(1 - V^2/\alpha)}$ and $p = \sqrt{12(V^2 - 1)}$. Similarly, using the simplest Padé approximation [17, 18], we obtain the equation

$$u_{tt} - (1/12)u_{\xi\xi tt} = (f(u_\xi))_\xi, \quad (14)$$

whose solitary wave solution is still (10)-(12) but now with $r = \sqrt{12(\alpha V^{-2} - 1)}$ and $p = \sqrt{12(1 - V^{-2})}$. All three QC theories have the same structure of the roots of the characteristic equations and therefore solutions differ only through the way r and p depend on V.

From Fig. 4 we see that the Taylor approximation (dashed curve) underestimates r and overestimates p, while the Padé approximation (dotted curve) overestimates r and underestimates p. A comparison of the velocity dependence of the transition point location z and amplitude of the solitary wave $w(0)$ generated by the three QC theories and by numerical solution of (6), (7) suggests that in the crossover regimes the $n = 1$ truncation provides a better overall approximation of the discrete problem than the conventional QC theories; see Fig. 5 and Fig. 6. The reason is that in these regimes the first roots of the characteristic equations are not close to the origin and are therefore captured rather poorly by the low-order asymptotic expansions around $k = 0$.

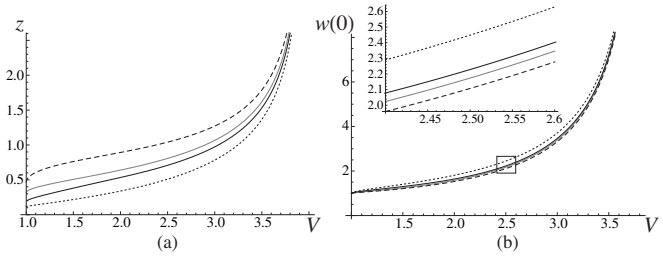

FIG. 5. The velocity dependence of (a) z and (b) amplitude of the solitary wave profiles (numerical solution of (6), (7), solid curves) compared with $n = 1$ (gray), Taylor (dashed) and Padé (dotted) QC approximations. Inset in (b) shows the enlarged view of the region inside the rectangle. Here $\alpha = 16$ and $w_c = 1$.

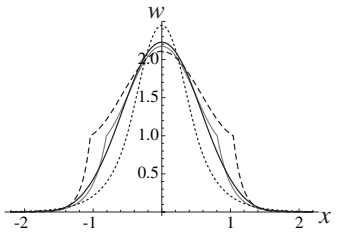

FIG. 6. Solitary wave profile at $V = 2.5$ (numerical solution of (6), (7), solid curve) compared with $n = 1$ (gray), Taylor (dashed) and Padé (dotted) QC approximations. Here $\alpha = 16$ and $w_c = 1$.

Both conventional QC theories work better at $V \gtrsim 1$ and $V \lesssim \sqrt{\alpha}$ but these two sonic limits are not physically relevant. Indeed, a realistic FPU potential with superquadratic growth would produce solutions with $w(0) \to 0$ for weak near-sonic waves instead of our $w(0) \to w_c$ and $V \to \infty$ for strong waves instead of our $V \to \sqrt{\alpha}$. Similar artifact is the divergence of the energy of solitary waves in both sonic limits (see Fig. 3a), and therefore the bilinear model with *fixed* w_c and α adequately describes only the intermediate (crossover) velocity range between QC and AC limits. The limiting regimes themselves can be captured through the appropriate double limits.

To reproduce the QC regime with $V \gtrsim 1$, the bilinear approximation needs to be adjusted so that $\alpha \to 1$ and $w_c \to 0$ as $V \to 1$. Consider, for example, a generic smooth interaction force satisfying $f(0) = 0$, $f'(0) = f''(0) = 1$ and construct a V-dependent bilinear approximation of $f(w)$ with $\alpha \approx 2V^2 - 1$ and $w_c \approx V^2 - 1$. It is then easy to show that when $V \gtrsim 1$ the first roots approach the origin, and the solitary wave solution in all three QC theories converge to the same KdV-type soliton.

V. THE ANTICONTINUUM LIMIT

The AC limit can be captured if $f(w)$ has a vertical asymptote, as in the hard-core models, so that the velocity V can grow to infinity. In this case we need to assume

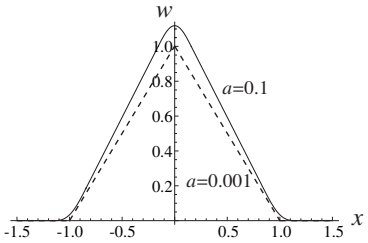

FIG. 7. The asymptotic almost triangular profiles of the strong solitary waves at large V and small a.

that $\alpha \to \infty$ and $V \to \infty$ while $V/\sqrt{\alpha} \to 0$. Indeed, when $\alpha > V^2 \gg 1$, the Fourier transform of $q(x)$ has the asymptotic representation $\hat{q}(k) \approx -4\sin^2(k/2)/(k^2V^2)$. For sufficiently small finite $a = V/\sqrt{2(\alpha-1)}$ the integral equation (7) can be then approximated by

$$-\frac{\alpha-1}{V^2}\int_{-z}^{z}(1-|x-s|)h(s)ds+h(x)=0, \quad |x|<z. \tag{15}$$

Differentiating (15) twice, we obtain

$$h''+\frac{h}{a^2}=0,$$

which yields

$$h(x)=\frac{1}{a}\sin\frac{x}{a}, \quad |x|<z, \quad z=\frac{\pi a}{2}. \tag{16}$$

Next, we observe that (6) can be written as

$$w(x)=A\int_{-z}^{z}\rho(x-s)h(s)ds, \tag{17}$$

where

$$\rho(x)=\int_{-\infty}^{x}q(s)ds \approx -\frac{1}{V^2}\int_{-\infty}^{x}(1-|s|)\theta(1-|s|)ds$$

at $V \gg 1$. Substituting this and (16) into (17) and using $w(\pi a/2) = w_c$ to find A, we obtain

$$w(x) \approx \frac{w_c}{1-\frac{\pi a}{2}}\times$$
$$\times\begin{cases} a\cos\frac{x}{a}+1-\frac{\pi a}{2}, & |x|\le\frac{\pi a}{2} \\ 1-|x|, & \frac{\pi a}{2}\le|x|\le 1-\frac{\pi a}{2} \\ \frac{1}{2}(1+\frac{\pi a}{2}-|x|-a\cos\frac{|x|-1}{a}), & 1-\frac{\pi a}{2}\le|x|\le 1+\frac{\pi a}{2} \\ 0, & |x|\ge 1+\frac{\pi a}{2}. \end{cases} \tag{18}$$

In the limit $a \to 0$ the profile $w(x)$ approaches the localized 'triangular' shape

$$w_\infty(x)=w_c(1-|x|)\theta(1-|x|). \tag{19}$$

Eq. (19) describes the AC regime when only one particle moves at a time [15]. The convergence to this limiting case is illustrated in Fig. 7. It is clear that neither of our three QC theories is applicable in this limit since it implies infinite values for either r (Padé approximation) or p (Taylor and $n = 1$ models).

VI. CONCLUSIONS

We constructed a non-integrable analog of the Toda family of solitary waves linking two universal asymptotic limits: weak delocalized QC solitary waves moving with near-sonic velocities and strong highly localized AC solitary waves where only one particle moves at a time. This new family of exact solutions of the FPU system makes fully explicit the contributions due to progressively smaller characteristic wavelengths. The solutions were obtained by a nontrivial application of the 'bilinearization' method which can be viewed as an extension of the classical 'linearization' approach. We showed that even the simplest truncation of the obtained series solution, accounting for the longest wave lengths, provides a better overall QC approximation of solitary waves than any of the conventional low-order QC models.

We provided numerical evidence of stability for some of the constructed solitary wave solutions. To access linear stability we need to consider small perturbations in

$$y_j(t) = w(x) + e^{\lambda V t}\Delta(x)$$

and linearize the governing equation (B1) around the solitary wave $w(x)$. Observing that $f'(w(x)) = 1 + (\alpha - 1)\theta(z - |x|)$, where z is known for given V, we obtain the following eigenvalue problem (quadratic in λ):

$$\begin{aligned} &V^2(\Delta''(x) - 2\lambda\Delta'(x) + \lambda^2\Delta(x)) - \Delta(x+1) + 2\Delta(x) \\ &- \Delta(x-1) - (\alpha-1)\Big(\theta(z - |x+1|)\Delta(x+1) \\ &- 2\theta(z-|x|)\Delta(x) + \theta(z-|x-1|)\Delta(x-1)\Big) = 0. \end{aligned} \tag{20}$$

Here $\Delta(x)$ tends to zero at infinity. In view of the Hamiltonian nature of the problem, a solitary wave is linearly stable if all eigenvalues λ are purely imaginary and semisimple. Study of the spectrum of the advance-delay differential operator in (20) will be part of the future work.

Appendix A: Derivation of the solution

To solve the linear integral equation (7), we follow [21–23] and extend the left hand side of the equation to the entire real axis:

$$\begin{aligned} (\alpha-1)\int_{-z}^{z} q(x-s)h(s)ds + h(x) \\ = \psi_-(x-z) + \psi_+(x+z), \quad -\infty < x < \infty. \end{aligned}$$

Here $\psi_\pm(x)$ are some unknown functions satisfying $\psi_-(x) \equiv 0$ for $x < 0$ and $\psi_+(x) \equiv 0$ for $x > 0$. Taking Fourier transform of both sides, we obtain

$$\frac{G(k)}{L(k)}H(k) = e^{ikz}\hat{\Psi}_+(k) + e^{-ikz}\hat{\Psi}_-(k), \tag{A1}$$

where $\hat{\Psi}_\pm(k)$ are Fourier transforms of $\psi_\pm(x)$. Using an infinite product representation [28] of the ratio $G(k)/L(k)$ in the generic case when all nonzero roots of $L(k) = 0$ and $G(k) = 0$ are simple [29], we have

$$\begin{aligned} &\frac{\alpha - V^2}{1 - V^2}\frac{\prod_{i=1}^{\infty}\left(1 - \frac{k^2}{\gamma_i^2}\right)}{\prod_{i=1}^{\infty}\left(1 - \frac{k}{\lambda_i^+}\right)\left(1 - \frac{k}{\lambda_i^-}\right)}H(k) \\ &= e^{ikz}\hat{\Psi}_+(k) + e^{-ikz}\hat{\Psi}_-(k). \end{aligned} \tag{A2}$$

If only finitely many roots $\pm\gamma_i$ $\lambda_i^\pm$, $i = 1, \ldots, n$, located within some strip $|\mathrm{Re}k| < l_n$ are included, (A2) is approximated by

$$\begin{aligned} &\frac{\prod_{i=1}^{n}(k^2 - \gamma_i^2)}{\prod_{i=1}^{n}(k - \lambda_i^+)\prod_{i=1}^{n}(k - \lambda_i^-)}H_n(k) \\ &= e^{ikz_n}\Psi_+^{(n)}(k) + e^{-ikz_n}\Psi_-^{(n)}(k), \end{aligned} \tag{A3}$$

where $H_n(k)$ and z_n approximate $H(k)$ and z, respectively, and

$$\Psi_\pm^{(n)}(k) = \frac{V^2 - 1}{\alpha - V^2}\prod_{i=1}^{n}\frac{|\gamma_i|^2}{|\lambda_i^+|^2}\hat{\Psi}_\pm(k). \tag{A4}$$

An analytic continuation argument [22, 23] then shows that

$$\begin{aligned} H_n(k) = \Bigg\{\sum_{m=1}^{n}\Big((-1)^{m-1}\prod_{i=1}^{n}(k - \lambda_i^+)e^{ikz_n} \\ + \prod_{i=1}^{n}(k - \lambda_i^-)e^{-ikz_n}\Big)c_m^{(n)}k^{m-1}\Bigg\}\Big/\prod_{i=1}^{n}(k^2 - \gamma_i^2), \end{aligned}$$

where we took into account the symmetry of the roots about the real and imaginary axes.

To determine the unknown coefficients $c_m^{(n)}$, we observe that as a Fourier transform of an L^2 function, the function $H_n(k)$ must be entire, which means that all roots of its denominator are also the roots of the numerator. This yields the following linear system for the coefficients $c_m^{(n)}$:

$$\sum_{m=1}^{n}(M_n)_{jm}(z_n)c_m^{(n)} = 0, \quad j = 1, \ldots, n, \tag{A5}$$

where $(M_n)_{jm}(z_n)$ are given by (9). The system of linear equations (A5) has a nontrivial solution if and only if the

determinant of the $n\times n$ matrix $M_n(z_n)$ with the entries $(M_n)_{jm}(z_n)$ is zero. Therefore we obtain an algebraic equation

$$\det M_n(z_n)=0, \tag{A6}$$

allowing one to find z_n. Once z_n is found, we can solve (A5) for $c_m^{(n)}$, which are determined up to an arbitrary multiplicative constant. We can then compute $H_n(k)$, which after some algebra reduces to [22]

$$H_n(k)=i\sum_{j=1}^{n}\frac{\prod_{i=1}^{n}(\gamma_j-\lambda_i^-)}{\gamma_j\prod_{i=1,\,i\neq j}^{n}(\gamma_j^2-\gamma_i^2)}\sum_{m=1}^{n}c_m^{(n)}\gamma_j^{m-1}\times \\ \times e^{-i\gamma_j z_n}\left(\frac{\sin((k+\gamma_j)z)}{k+\gamma_j}-\frac{\sin((k-\gamma_j)z)}{k-\gamma_j}\right), \tag{A7}$$

where we used the symmetry of the roots. This yields

$$h_n(x)=\sum_{j=1}^{n}\frac{\sin(\gamma_j x)e^{-i\gamma_j z_n}\prod_{i=1}^{n}(\gamma_j-\lambda_i^-)}{\gamma_j\prod_{i=1,\,i\neq j}^{n}(\gamma_j^2-\gamma_i^2)}\sum_{m=1}^{n}c_m^{(n)}\gamma_j^{m-1}. \tag{A8}$$

The normalization condition $\int_0^{z_n}h_n(x)dx=1$ then selects a unique set of coefficients $c_m^{(n)}$ and yields the approximate solution $h_n(x)$ of the integral equation. The exact solution of (7) and the value of z are obtained in the limit $n\to\infty$.

We now show how the knowledge of $h_n(x)$ can be used to recover the strain field $w_n(x)$. Substituting into (6) the truncated approximation of $G(k)H(k)/L(k)$ that includes only the first $4n$ roots and recalling (A3), (A4), we obtain

$$w_n(x)=\frac{A_n}{2\pi i(\alpha-1)}\frac{\alpha-V^2}{1-V^2}\left(\prod_{i=1}^{n}|\gamma_i|\right)^{-2}\times \\ \times\left(\prod_{i=1}^{n}\lambda_i^+\int_\Gamma\frac{\sum_{m=1}^{n}(-1)^{m-1}c_m^{(n)}k^{m-1}}{k\prod_{i=1}^{n}\left(1-\frac{k}{\lambda_i^-}\right)}e^{ik(x+z_n)}dk\right. \\ \left.+\prod_{i=1}^{n}\lambda_i^-\int_\Gamma\frac{\sum_{m=1}^{n}c_m^{(n)}k^{m-1}}{k\prod_{i=1}^{n_+}\left(1-\frac{k}{\lambda_i^+}\right)}e^{ik(x-z_n)}dk\right) \\ +\frac{A_n}{\alpha-1}\int_x^{z_n}h_n(x)dx. \tag{A9}$$

Here the contour Γ goes along the real line everywhere except a small neighborhood of $k=0$, where it goes above the origin in order to resolve the simple pole at $k=0$. In addition to this singularity on the real axis, the first integrand has simple poles at $k=\lambda_i^-$ in the lower half $\mathrm{Im}k<0$ of the complex plane, and the second integrand has simple poles at $k=\lambda_i^+$ in the upper half-plane $\mathrm{Im}k>0$. Applying the residue theorem, recalling (A8) and using $w_n(\pm z_n)=w_c$ to determine A_n, we obtain

$$w_n(x)=w_c\left(1-\frac{V^2-1}{c_1^{(n)}(\alpha-V^2)}\sum_{j=1}^{n}\frac{\prod_{i=1}^{n}\left(1-\frac{\gamma_j}{\lambda_i^-}\right)}{\prod_{i=1,\,i\neq j}^{n}\left(1-\frac{\gamma_j^2}{\gamma_i^2}\right)}\times \right. \\ \left.\times e^{-i\gamma_j z_n}\sum_{m=1}^{n}c_m^{(n)}\gamma_j^{m-1}(\cos(\gamma_j x)-\cos(\gamma_j z_n))\right) \tag{A10}$$

for $|x|<z_n$ and

$$w_n(x)=\frac{w_c}{c_1^{(n)}}\sum_{j=1}^{n}\frac{\sum_{m=1}^{n}c_m^{(n)}(\lambda_j^+)^{m-1}}{\prod_{i=1,\,i\neq j}^{n}\left(1-\frac{\lambda_j^+}{\lambda_i^+}\right)}e^{i\lambda_j^+(|x|-z_n)} \tag{A11}$$

for $|x|>z_n$. The continuity at $x=\pm z_n$ is automatically ensured by the fact that the sum of residues of the first integrand of (A9) at $x=-z_n$ and the second integrand at $x=z_n$ at all poles equals zero, meaning that

$$c_1^{(n)}-\sum_{j=1}^{n}\frac{\sum_{m=1}^{n}c_m^{(n)}(\lambda_j^+)^{m-1}}{\prod_{i=1,\,i\neq j}^{n}\left(1-\frac{\lambda_j^+}{\lambda_i^+}\right)}=0.$$

Equations (A8) and (A10) together with the constraint $\int_0^{z_n}h_n(x)dx=1$ yield an explicit formula for the amplitude of the solitary wave:

$$w_n(0)=w_c\left(1+\frac{V^2-1}{\alpha-V^2}\left(\prod_{i=1}^{n}|\gamma_i|\right)^2\left(c_1^{(n)}\prod_{i=1}^{n}\lambda_i^-\right)^{-1}\right). \tag{A12}$$

The expressions (A10), (A11), with coefficients $c_m^{(n)}$, $m=1,\dots,n$, solving the linear system (A5), and with z_n satisfying the nonlinear equation (A6), furnish an approximate solution of the problem (2), (3). In the limit

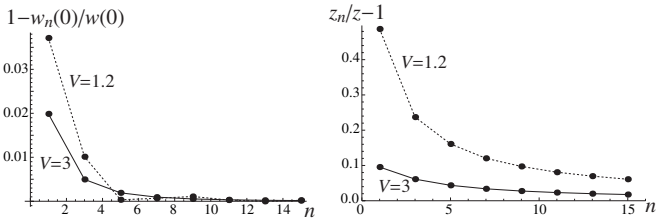

FIG. 8. The errors due to finite truncation of the series at $\alpha=16$ and $w_c=1$. Here $w_n(0)$ and z_n were obtained from (A12) and (A6), respectively, and the reference values $w(0)$ and z were computed numerically using trapezoidal approximation of (7) and (17).

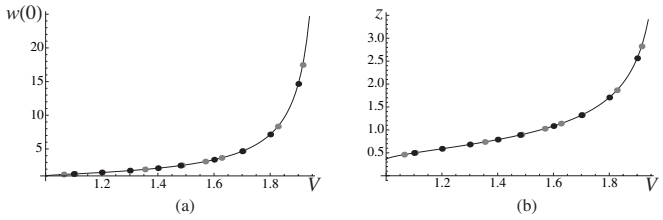

FIG. 9. (a) Amplitude-velocity relation and (b) the corresponding $z(V)$ at $\alpha = 4$ and $w_c = 1$ obtained from the semi-analytical solution (solid curves) and numerical simulation of (B1) with initial conditions (B2) (black circles) and (B3) (gray circles).

$n \to \infty$ we obtain the exact solution (8) with

$$a_0 = w_c\Bigg(1 + \frac{V^2-1}{\alpha - V^2}\lim_{n\to\infty}\frac{1}{c_1^{(n)}}\sum_{j=1}^{n}\frac{\prod_{i=1}^{n}\left(1-\frac{\gamma_j}{\lambda_i^-}\right)}{\prod_{i=1,\,i\neq j}^{n}\left(1-\frac{\gamma_j^2}{\gamma_i^2}\right)}\times$$
$$\times\, e^{-i\gamma_j z_n}\sum_{m=1}^{n} c_m^{(n)}\gamma_j^{m-1}\cos(\gamma_j z_n)\Bigg), \tag{A13}$$

$$a_j = -w_c\frac{V^2-1}{\alpha - V^2}\lim_{n\to\infty}\frac{1}{c_1^{(n)}}\frac{\prod_{i=1}^{n}\left(1-\frac{\gamma_j}{\lambda_i^-}\right)}{\prod_{i=1,\,i\neq j}^{n}\left(1-\frac{\gamma_j^2}{\gamma_i^2}\right)}\times \tag{A14}$$
$$\times\, e^{-i\gamma_j z_n}\sum_{m=1}^{n} c_m^{(n)}\gamma_j^{m-1}$$

and

$$b_j = w_c\lim_{n\to\infty}\frac{e^{-i\lambda_j^+ z_n}}{c_1^{(n)}}\frac{\sum_{m=1}^{n} c_m^{(n)}(\lambda_j^+)^{m-1}}{\prod_{i=1,\,i\neq j}^{n}\left(1-\frac{\lambda_j^+}{\lambda_i^+}\right)}. \tag{A15}$$

Numerical results shown in Fig. 2 and in Fig. 8 illustrate convergence to the exact solution.

Appendix B: Numerical evidence of stability for some of the solitary wave solutions

To study stability of the obtained solitary wave solutions we consider the initial value problem for the original discrete system

$$\ddot{y}_j = f(y_{j+1}) - 2f(y_j) + f(y_{j-1}) \tag{B1}$$

with zero boundary conditions.

The first type of initial conditions was constructed from the solitary wave solutions $y_j(t) = w(x)$, $x = j - Vt$ computed numerically at a given V:

$$y_j(0) = w(j - j_0), \quad \dot{y}_j(0) = -Vw'(j - j_0), \tag{B2}$$

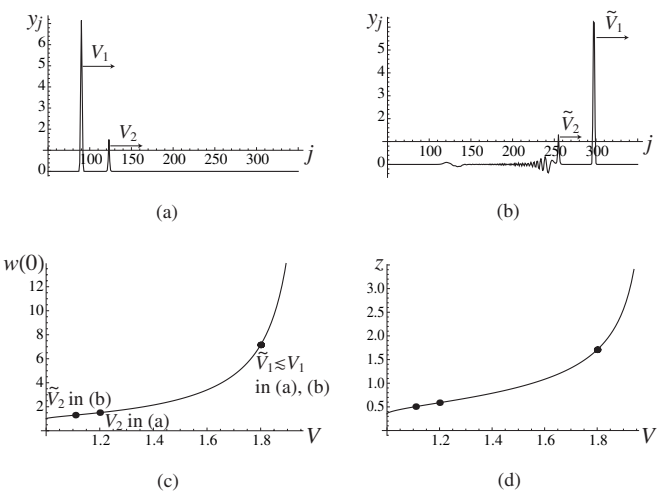

FIG. 10. Numerical simulations showing collision of the solitary waves: (a) a faster ($V_1 = 1.8$) and a slower ($V_2 = 1.2$) waves moving to the right before the collision ($t = 30$); (b) after the collision ($t = 145$) the faster wave propagates with $\tilde{V}_1 \approx 1.8$, while the slower wave slows down to $\tilde{V}_2 \approx 1.1$. The corresponding amplitude and z values are shown by circles in (c) and (d), respectively.

where we set $j_0 = 100$. We found that at $1 < V < V_{cr}$, where V_{cr} depends on α (e.g. $V_{cr} \approx 1.05$ at $\alpha = 4$), the amplitude of the initial perturbation decreases with time and at large times the strain localizes in the first linear regime ($y_j < w_c$). At $V_{cr} < V < \sqrt{\alpha}$ in (B2) the numerical solution converges to a steadily propagating solitary wave. We found that the velocities, amplitudes and the values of z of the attracting solitary waves were very close to the ones in the initial conditions, suggesting stability of the corresponding traveling wave solutions. The results are presented by black circles in Fig. 9.

To probe stability of the solitary waves in a larger domain, we also considered the second type of initial conditions with a localized initial profile

$$y_j(0) = A_0\exp\left(-\frac{1}{2}\left|j - \frac{M}{2}\right|^2\right), \quad \dot{y}_j(0) = 0, \tag{B3}$$

where the amplitude A_0 served as a parameter. At sufficiently small amplitudes (e.g. $A_0 < 1.94$ at $\alpha = 4$), the long-time behavior corresponded again to a solution of the linear equation with $y_j < w_c$. For larger A_0 the initial data evolved into two solitary waves propagating towards different ends of the chain. A broad agreement in the whole range of velocities $V_{cr} < V < \sqrt{\alpha}$ can be seen on the amplitude-velocity relation shown in Fig. 9, where the results numerical solutions with initial conditions (B3) are presented by gray circles.

In both sets of simulations the threshold velocity $V = V_{cr}$ at which the stability changes corresponds to the minimum of the energy (1) as the function of V, with solitary waves stable along the increasing portion of $\mathcal{H}(V)$ ($V > V_{cr}$) and unstable otherwise; see Fig. 3a.

We now report the results of two collision tests. In the first test, illustrated in Fig. 3b, two solitary waves travel-

ing towards each other with the speed $V = 1.6$ were chosen as the initial condition. After the collision both waves continued propagating with only slightly lower velocities and with some oscillations developing in the wake. This numerical experiment shows that the collision is not fully elastic, as expected since the system is non-integrable. In the second test the initial conditions involved two waves moving in the same direction but with different velocities, a faster wave, with $V_1 = 1.8$, behind, and a slower wave, with $V_2 = 1.2$, ahead; see Fig. 10a. In this case after the faster wave overtook the slower one, it continued propagating with almost the same speed as before, while the slower wave's velocity decreased to $\tilde{V}_2 \approx 1.1$, and a dispersive wave developed behind it, as can be seen in Fig. 10b. Once again, the collision was not completely elastic even though solitary wave profiles have been rebuilt after the collision. The values of amplitude and z for the two collision experiments are shown in Fig. 10(c,d).

ACKNOWLEDGMENTS

Support from the NSF grant DMS-1007908 (A.V.) is gratefully acknowledged.

[1] T. Dauxois and M. Peyrard, *Physics of Solitons* (Cambridge University Press, 2010).
[2] M. Toda, *Theory of nonlinear lattices* (Springer, Berlin, 1981).
[3] J. A. D. Wattis, J. Phys. A **29**, 8139 (1996).
[4] G. Iooss, Nonlinearity **13**, 849 (2000).
[5] S. Sen, J. Hong, J. Bang, E. Avalos, and R. Doney, Phys. Rep. **462**, 21 (2008).
[6] J. C. Eilbeck and R. Flesch, Phys. Lett. A **149**, 200 (1990).
[7] T. Mizumachi and N. Tzvetkov, arXiv preprint arXiv:1403.5321 (2014).
[8] S. Flach, Y. Zolotaryuk, and K. Kladko, Phys. Rev. E **59**, 6105 (1999).
[9] E. Fermi, J. Pasta, and S. Ulam, *Studies of nonlinear problems*, Tech. Rep. LA-1940 (Los Alamos Scientific Laboratory, 1955).
[10] B. Lippmann and J. Schwinger, Phys. Rev. **79**, 469 (1950).
[11] Z. Hasin and S. Strickman, J. Mech. Phys. Solids **10**, 335 (1962).
[12] N. J. Zabusky and M. D. Kruskal, Phys. Rev. Lett. **15**, 240 (1965).
[13] G. Friesecke and R. L. Pego, Nonlinearity **12**, 1601 (1999).
[14] O. A. Druzhinin and L. A. Ostrovskii, Phys. Lett. A **160**, 357 (1991).
[15] G. Friesecke and K. Matthies, Physica D **171**, 211 (2002).
[16] J. A. D. Wattis, J. Phys. A **26**, 1193 (1993).
[17] M. A. Collins, Chem. Phys. Lett. **77**, 342 (1981).
[18] P. Rosenau, Phys. Lett. A **118**, 222 (1986).
[19] N. Flytzanis, S. Crowley, and V. Celli, J. Phys. Chem. Solids **38**, 539 (1977).
[20] A. Vainchtein, J. Mech. Phys. Solids **58**, 227 (2010).
[21] M. P. Ganin, Izv. Vyssh Ucheb. Zaved. Mat. **2** (1963).
[22] B. V. Pal'tsev, Math USSR Izvestija **6**, 587 (1972).
[23] J. I. Ljubarskii, Math USSR Izvestija **11**, 583 (1977).
[24] Here we assume the roots are all simple, which is true for generic values of V and α.
[25] N. G. Vakhitov and A. A. Kolokolov, Radiophys. Quant. Electr. **16**, 783 (1973).
[26] S. F. Mingaleev, Y. B. Gaididei, and F. G. Mertens, Phys. Rev. E **61**, R1044 (2000).
[27] L. Truskinovsky and A. Vainchtein, Cont. Mech. Thermodyn. **18**, 1 (2006).
[28] L. I. Slepyan, Mech. Solids **16**, 101 (1982).
[29] One can show that the nonzero roots of $G(k) = 0$ are simple for any $\alpha > 1$ and $1 < V < \sqrt{\alpha}$ such that $G(k)$ and $G'(k)$ do not vanish simultaneously for some real positive k, while the nonzero roots of $L(k) = 0$ are always simple in this parameter domain.